

LightTact: A Visual–Tactile Fingertip Sensor for Deformation-Independent Contact Sensing

Changyi Lin^{*1}, Boda Huo^{*1}, Mingyang Yu¹, Emily Ruppel², Bingqing Chen², Jonathan Francis^{1,2}, Ding Zhao¹

<https://linchangyi1.github.io/LightTact>

Abstract—Contact often occurs without macroscopic surface deformation, such as during interaction with liquids, semi-liquids, or ultra-soft materials. Most existing tactile sensors rely on deformation to infer contact, making such light-contact interactions difficult to perceive robustly. To address this, we present LightTact, a visual-tactile fingertip sensor that makes *contact directly visible* via a deformation-independent, optics-based principle. LightTact uses an ambient-blocking optical configuration that suppresses both external light and internal illumination at non-contact regions, while transmitting only the diffuse light generated at true contacts. As a result, LightTact produces high-contrast raw images in which non-contact pixels remain near-black (mean gray value < 3) and contact pixels preserve the natural appearance of the contacting surface. Built on this, LightTact achieves accurate pixel-level contact segmentation that is robust to material properties, contact force, surface appearance, and environmental lighting. We further integrate LightTact on a robotic arm and demonstrate manipulation behaviors driven by extremely light contact, including water spreading, facial-cream dipping, and thin-film interaction. Finally, we show that LightTact’s spatially aligned visual-tactile images can be directly interpreted by existing vision-language models, enabling resistor value reasoning for robotic sorting.

I. INTRODUCTION

Contact occurs throughout physical interactions between robots and their environments, for example, between fingertips and objects during manipulation or between feet and terrain during locomotion. To perform such interactions safely, precisely, and robustly, robots must be able to detect and localize contact [1, 2]. Vision-based tactile sensors (VBTSSs) have gained prominence in recent years due to their high spatial resolution and low cost [3, 4, 5, 6]. However, most VBTSSs sense contact *indirectly* by observing macroscopic deformation of a soft surface [7, 8, 9, 10, 11]. This deformation-dependent mechanism fundamentally requires measurable indentation to generate informative tactile signal. In contrast, many real-world interactions involve *light* contacts that induce little or no surface deformation. Examples include interactions with liquids or semi-liquids, and gentle contacts with extremely soft or thin materials. Such scenarios are common in everyday tasks, such as spreading water on a tabletop, dipping facial cream, or detecting a sheet of food film, but they remain challenging for deformation-based tactile sensors.

Several sensors attempt to bypass deformation by using frustrated total internal reflection (TIR) to highlight the contact regions of a transparent medium [12, 13, 14, 15]. However,

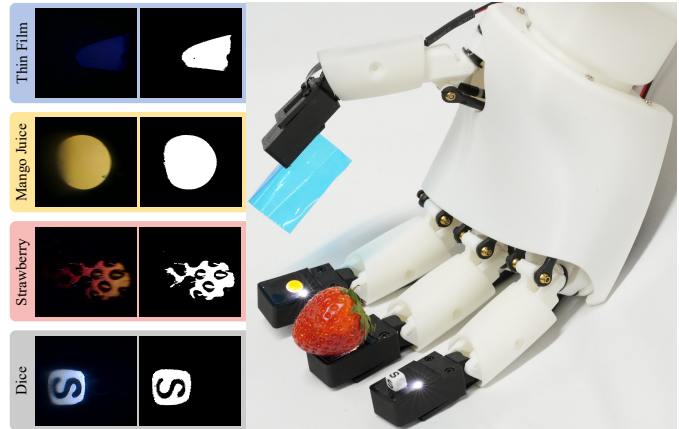


Figure 1. LightTact provides direct, pixel-level contact sensing across liquids, ultra-soft materials, and rigid objects, without requiring a minimum contact force. Its optical design produces high-contrast raw images in which non-contact pixels remain near-black, while contact pixels preserve the natural appearance of the contacting surface. LightTact is fingertip-sized and can be integrated into dexterous hands such as Amazing Hand [16].

ambient illumination and reflections from non-contact regions can also enter the camera, seriously corrupting the highlighted contact signal. As a result, TIR-based sensors typically function reliably only with monochromatic objects or under dark, tightly controlled environments—conditions incompatible with robotic tactile perception in everyday, unstructured settings. Thus, building a tactile sensor that can robustly detect contact *without* relying on surface deformation remains an open challenge.

To address this challenge, we introduce LightTact, a compact fingertip visual–tactile sensor that achieves *direct, optics-based* contact detection independent of surface deformation (Fig. 1). The key innovation is our dedicated optical configuration that entirely suppresses both external light and internal illumination at non-contact regions, while allowing only the diffuse light generated at true contacts to reach the camera. This design fundamentally changes how contact is encoded in the raw sensor image, enabling three core properties:

- **High-contrast raw images.** LightTact captures raw images with naturally high-contrast contact representation: non-contact pixels remain near-black (intensity < 2), while contacting regions appear relatively bright.
- **Robust pixel-level contact segmentation.** Supported by the inherent optical isolation, for the first time, LightTact achieves pixel-level contact segmentation that is robust to material properties, contact forces, surface appearance,

^{*} Equal contribution

¹ Carnegie Mellon University

² Bosch Center for Artificial Intelligence (BCAI)

and environmental lighting.

- **Aligned visual–tactile multimodality.** The bright pixels simultaneously encode the localized visual appearance of the object and the contact region of the sensor surface, producing a naturally aligned multimodal signal suitable for robot learning and high-level reasoning.

Leveraging these properties, we integrate LightTact into a robotic system and demonstrate manipulation capabilities that remain difficult or inaccessible for existing tactile sensors. These include reliable interaction with liquids, semi-liquids, and extremely soft materials, as well as fine-grained sorting of tiny objects by directly prompting LightTact images to vision–language models. Together, these results indicate that LightTact enables a new class of manipulation behaviors by providing direct, optics-based sensing of true physical contact.

In summary, our contributions are as follows:

- We propose an ambient-blocking optical layout that theoretically isolates all external and internal illumination from non-contact regions, enabling intuitive contact visualization without relying on deformation.
- We introduce LightTact, a compact fingertip visual-tactile sensor that achieves robust contact segmentation with minimal computation cost.
- We systematically evaluate LightTact across diverse materials, contact areas, and lighting conditions, and report its success and failure cases.
- We demonstrate that LightTact unlocks manipulation capabilities that require reliable detection of light contact, and supports multimodal reasoning by directly prompting LightTact images to vision–language models.

II. RELATED WORK

We review prior work in two aspects most relevant to this paper: (1) *robust contact sensing and segmentation* in vision-based tactile sensors (VBTSSs), and (2) *simultaneous visual–tactile sensing* for robotic manipulation.

A. Contact Sensing with Vision-Based Tactile Sensors

Vision-based tactile sensors (VBTSSs) use internal cameras to capture visualized tactile signals, offering high spatial sensitivity at low cost. However, most existing VBTSSs detect contact *indirectly* by observing macroscopic deformation of a soft sensing surface. Common approaches include tracking painted markers [8, 10, 17, 18, 11, 19], observing magnified reflective patterns [20, 21], or measuring luminance variations of reflective layers [7, 9]. Fundamentally, these approaches require visible surface deformation, which imposes three constraints: the surface must be soft, the contacting object must be relatively harder, and the applied force must exceed a detectable deformation threshold. These requirements not only fix the sensor to a soft surface, but also severely limit its ability to perceive *light contacts* that do not generate measurable indentation, such as touching water, facial cream, or thin films.

To decouple sensing from mechanical deformation, several sensors [12, 13, 14, 15] apply total internal reflection (TIR) within a transparent medium. When an object contacts the

medium, local frustration of TIR occurs, reflecting additional light toward the camera and thereby highlighting contact regions. However, this highlighting strategy is highly sensitive to ambient light. External light, reflections from non-contact portions of the object, and internal LED illumination can all enter the camera through non-contact regions, interfering with or overwhelming the intended TIR-based contact signal. As a result, these systems operate reliably only with monochromatic objects or under controlled, dark environments.

In contrast, LightTact completely suppresses both external and internal illumination at non-contact regions while capturing only the diffuse light generated at true contacts. This ensures that non-contact pixels remain near-black in raw images, enabling, for the first time, robust pixel-level contact segmentation across diverse lighting conditions and object appearances.

Similar objectives of reducing interference from external light have appeared in non-robotic optical devices, such as the Wyman–White fingerprint imager [22] and the Drawing Prism [23]. However, these systems were designed for static fingerprint capture or artistic tracing, where requirements are substantially more relaxed. They do not enforce strict darkness of non-contact pixels, assume controlled lighting conditions, or restrict the types of interacting objects. As a result, they rely on bulky geometries, dark environments, and even a thin liquid layer to eliminate air gaps. Such conditions are incompatible with robotic tactile perception, where sensors must operate reliably in dynamic, unconstrained daily environments.

B. Visual-Tactile Multimodal Sensing

A prevalent strategy for combining visual and tactile modalities is to paint markers on a transparent gel [8, 24, 25, 26, 27, 28, 29]. However, this approach provides only sparse motion cues and inherently occludes visual information at marker locations. To preserve full-pixel visibility, alternative methods utilize translucent coatings paired with illumination switching [30, 31, 32], but they support only one modality at a time. While TIR-based designs [12, 13, 14, 15] can theoretically provide visual information, the bright internal illumination required for tactile sensing often causes overexposure, degrading the external visual features. In contrast, LightTact achieves the simultaneous acquisition of robust pixel-level contact segmentation and natural visual appearance using a single camera, ensuring both modalities are spatially and temporally aligned by construction.

III. METHODOLOGY

Our goal is to design LightTact as a robotic tactile sensor capable of reliable, pixel-level contact segmentation across diverse objects and lighting conditions. To this end, we first introduce a novel optical layout and sensing principle and analyze its theoretical behavior in Section III-A. We then present how LightTact realizes this principle within a compliant, fingertip-scale form factor suitable for robotic integration in Section III-B. Following, we describe the key fabrication steps for constructing LightTact in Section III-C.

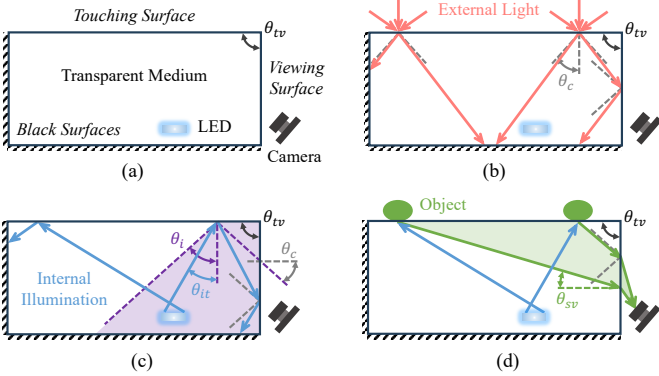


Figure 2. Optical layout and sensing principle of LightTact. (a) Core components: a transparent medium with a touching and viewing surface, an internal LED, and a camera. (b) External light entering through non-contact regions is rejected by refraction followed by total internal reflection (TIR). (c) Internal LED illumination reflecting from non-contact regions is also rejected by TIR when the LED is placed within the purple area to satisfy $\theta_{it} < \theta_i$. (d) At true contact, the air gap is removed and the contacting surface produces diffuse reflection. A subset of these rays reaches the viewing surface with incidence $< \theta_c$ and refracts toward the camera.

Finally, we introduce our algorithms for contact segmentation in Section III-D.

A. Optical Layout and Sensing Principle

Figure 2 (a) shows the core optical elements of LightTact: a transparent medium that interacts with external objects, an internal LED for illumination, and a camera that observes light exiting the medium. Two surfaces of the medium play distinct optical roles: the *touching surface*, where contact occurs, and the *viewing surface*, through which light exits toward the camera. The remaining surfaces are coated matte-black to absorb any light that reaches them. At the touching surface, combining two light sources (external light and internal illumination) with two region types (contact vs. non-contact) produces three relevant light behaviors for non-luminous objects: (1) external light incident on non-contact regions, (2) internal illumination incident on non-contact regions, and (3) internal illumination scattered at contact regions.

Our design objective is to obtain deformation-independent contact segmentation directly from the raw image. To achieve this, the optical layout must *completely suppress* both external and internal light at all non-contact regions, while *transmitting* only light generated at true contacts. A central mechanism enabling this property is the *nonparallel wedge geometry*: the touching and viewing surfaces form an angle θ_{tv} rather than being parallel. This geometry forces the three classes of light above to follow fundamentally different optical paths, allowing only the contact-scattered light to transmit through the viewing surface. Table I summarizes these behaviors, and the following paragraphs explain each in detail.

a) *External light rejection at non-contact regions*: As illustrated in Fig. 2 (b), external rays approach the touching surface from a wide range of directions. The sensing region corresponds to the span between the two depicted ray bundles. When external light enters the medium through non-contact

Table I
OPTICAL BEHAVIORS AND GEOMETRIC CONDITIONS FOR EACH LIGHT–SURFACE INTERACTION.

| Source | Region | Optical behavior at surfaces | | Design condition |
|----------|---------|------------------------------|-----------------|--|
| | | Touching surface | Viewing surface | |
| External | Non-con | Refraction | TIR | $\theta_{tv} > 2\theta_c$ |
| Internal | Non-con | Specular reflection | TIR | $\forall \theta_{it} < \theta_{tv} - \theta_c$ |
| Internal | Contact | Diffuse reflection | Refraction | $\theta_{tv} < \frac{\pi}{2} + \theta_c$ |

areas, it refracts into the medium at angles below the critical angle θ_c due to the air–medium index difference. A portion of these refracted rays then propagate toward the viewing surface. By choosing a sufficiently large wedge angle ($\theta_{tv} > 2\theta_c$), all such rays arrive at the viewing surface with incidence $> \theta_c$, causing them to undergo total internal reflection (TIR) and redirecting them toward the black surfaces. Consequently, no external light from non-contact regions reaches the camera.

b) *Internal illumination rejection at non-contact regions*: Internal LED illumination should contribute to the image only at true contacts. As shown in Fig. 2(c), LED rays that reflect specularly off non-contact regions of the touching surface, must also reach the viewing surface with incidence $> \theta_c$ to ensure TIR. This is guaranteed by constraining the LED position: the LED must lie entirely within the purple admissible region such that all emitted rays satisfy $\theta_{it} < \theta_i = \theta_{tv} - \theta_c$. Under this placement rule, every specularly reflected LED ray is rejected by TIR at the viewing surface, ensuring that no internal light leaks into the camera through non-contact regions.

c) *Appearance capture at contact regions*: When an object touches the medium, the air gap disappears and the contacting surface produces diffuse reflection of the LED illumination (Fig. 2(d)). This generates a wide angular spread of rays, which can reach the viewing surface with incidence $\theta_{sv} \in (\theta_{tv} - \frac{\pi}{2}, \frac{\pi}{2})$. To observe the contacting surface, a subset of these scattered rays must refract through the viewing surface and reach the camera. This requires that the incidence range $(\theta_{tv} - \frac{\pi}{2}, \frac{\pi}{2})$ intersects the transmissible range $(-\theta_c, \theta_c)$, which is satisfied when $\theta_{tv} < \frac{\pi}{2} + \theta_c$. Under this condition, a subset of diffuse-reflection rays transmits within the green regions and enters the camera, revealing the natural local appearance of the object. Meanwhile, all non-contact pixels remain black, producing a clean, high-contrast raw image that enables deformation-independent contact segmentation.

Our optical layout ensures that no light from non-contact regions reaches the camera by enforcing the condition $\theta_{tv} > 2\theta_c$, which guarantees that all such rays are rejected by the viewing surface under TIR. Strictly speaking, $\theta_{tv} > 2\theta_c$ is not the only possible configuration. If $\theta_{tv} < 2\theta_c$, the camera could, in principle, be positioned so that any rays refracted through the viewing surface from non-contact regions fall outside its field of view. However, this alternative requires placing the camera significantly farther from the touching surface and introduces additional complications: rays refracted through the viewing surface may require additional black surfaces to prevent unintended reflections back toward the camera.

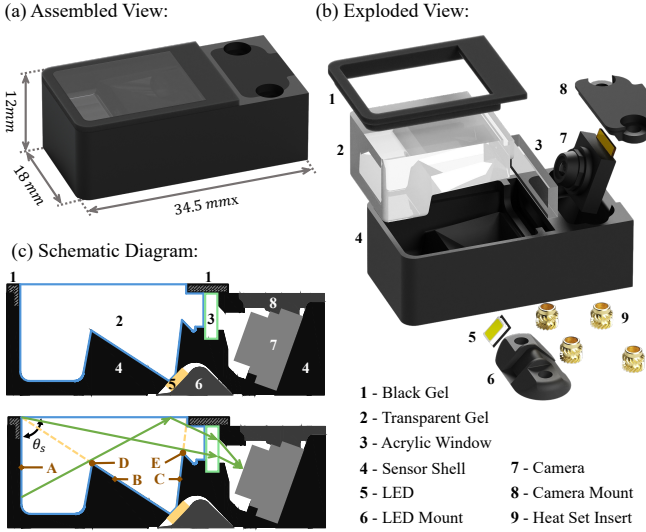


Figure 3. Design of LightTact. (a) Assembled view of LightTact. (b) Components of LightTact illustrated in exploded view. (c) Schematic diagram of LightTact.

We therefore adopt the simpler and more robust condition $\theta_{tv} > 2\theta_c$ as our default configuration. A detailed analysis of camera-placement alternatives and their limitations is provided in Appendix V-A.

B. Sensor Design

As shown in Fig. 3 (a), LightTact is extremely compact, with a fingertip-scale size of only $34.5\text{mm} \times 18\text{mm} \times 12\text{mm}$. Figures 3 (b) and (c) illustrate the internal assembly, which mirrors the optical system described in Section III-A: a transparent medium (2, 3), an internal LED (5), and a camera (7), all housed within a rigid shell (8), a surrounding black gel layer (1), and lightweight mounts (4, 6). The following paragraphs describe each component in detail.

Transparent gel and acrylic window. For most robotic applications, the touching surface should be soft to enable compliant physical interaction. Importantly, this softness is a design preference rather than a sensing requirement, since our optical principle does not rely on macroscopic deformation. However, a fully soft transparent medium would cause the viewing surface to deform under load, producing image distortion. To prevent this, the transparent medium combines a soft transparent silicone gel (for soft touching surface) with a rigid acrylic window (for rigid viewing surface). Both materials have similar refractive indices (≈ 1.45), which yields a critical angle of $\theta_c \approx 43^\circ$. To satisfy the conditions derived in Section III-A, namely $\theta_{tv} > 2\theta_c \approx 86^\circ$ for suppressing all non-contact light, and $\theta_{tv} < 90^\circ + \theta_c \approx 133^\circ$ for transmitting contact-scattered light, we set the touching and viewing surfaces to be perpendicular.

LED and camera. Internal illumination is provided by a single 2835-SMD LED. The LED is mounted at an oblique angle (approximately 45°) to provide more uniform lighting across the touching surface. Imaging is performed by a compact

UVC camera (based on OV5693) with a 120° field of view, placed close to the transparent medium to maintain the overall compactness of the sensor. Both the LED and the camera are fastened with lightweight mounts, which attach to the sensor shell using M2 screws and heat-set inserts.

Sensor shell. The sensor shell not only fixes the optical components in their required poses, but also constrains three critical geometric-optical properties: the transparent gel's shape, the LED's illumination range, the camera's effective viewing range. These design aspects are summarized below.

a) Transparent gel geometry: Although the sensor shell is built from black material to approximate the ideal “light-absorbing” boundaries assumed in Section III-A, real materials cannot completely absorb incident light. As indicated in Fig. 3 (c), the black surface labeled A may still reflect light toward the camera through non-contact regions. To suppress this effect, surface A is designed to be vertical ($\theta_s = \frac{\pi}{2}$), which minimizes the likelihood of specular reflections coupling into the viewing path. For certain robotic applications that require entering narrow spaces, the sensor may adopt a wedge-shaped profile. We analyze the configuration $\theta_s < \frac{\pi}{2}$ and its optical consequences in detail in Appendix V-C.

b) LED illumination range: To prevent the LED from directly illuminating surface A, the shell incorporates two baffles (surfaces B and C) that restrict the emission range of the LED. Although taller baffles improve shielding, their height is limited for two reasons: 1) If surface A extends above point D, the protruding inclined region will be directly illuminated and significantly increase the amount of light entering the camera via non-contact surface. 2) If surface B exceeds point E, it blocks a portion of the diffuse-reflection light from contact regions of the left side of the touching surface.

c) Camera's effective viewing range: The shell further restricts the camera's field of view so that only the touching surface is observable. If the camera could see outside this region, additional stray light, such as the scattered light from the rough top or bottom surfaces of the acrylic window, could interfere with the pixels corresponding to the touching surface.

Black gel. To preserve compliance over the entire contact area, the soft black gel is added around the perimeter of the transparent gel, forming a smooth transition between the touching surface and the rigid shell. It also covers the top surface of the acrylic window, which cannot function as part of the touching surface due to its rigidity and roughness.

C. Sensor Fabrication

Fabricating the two gel layers of LightTact requires several auxiliary molds and temporary inserts to form accurate internal boundaries, as illustrated in Fig. 4.

Transparent gel. The transparent gel is cast from Silicones Inc® XP-565 silicone (mixing ratio 10:1, shore A27), chosen for its high clarity and stable mechanical properties. The acrylic window, laser-cut from 1.5mm acrylic sheet, is installed inside the 3D-printed black PLA shell. To create a sealed cavity for casting the transparent silicone, the LED

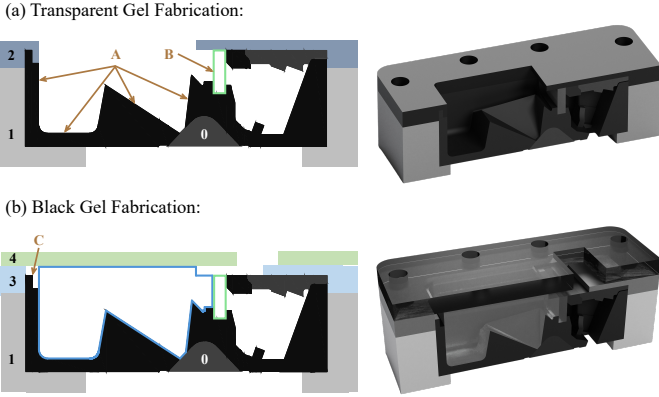


Figure 4. Gel fabrication for LightTact. (a) Casting of the transparent gel. The sensor shell, the mold 0, and the acrylic window together form a closed container. (b) Casting of the black gel. The top acrylic mold 4 ensures that the black gel cures to a uniform height around the transparent gel.

mount geometry is temporarily modified by filling its original LED recess with a solid insert (labeled 0 in Fig. 4(a)) so that no silicone leaks into the LED compartment. Two additional 3D-printed molds (labeled 1 and 2) are stacked around the shell to reserve the perimeter region occupied by the future black gel.

Before pouring the transparent silicone, a high-absorption black pigment (Black 2.0) is brushed onto the relevant inner surfaces of the shell (labeled A in Fig. 4(a)) to more closely approximate the idealized absorbing boundaries assumed in Section III-A. To ensure strong bonding between the acrylic window and the cured silicone, a thin layer of silicone adhesive (Smooth-On® Sil-Poxy) is brushed onto the acrylic face that will contact the gel (labeled B in Fig. 4(a)). After preparing these surfaces, degassed XP-565 silicone is poured into the cavity until it completely fills the interior of the shell. It takes about 4 hours for the silicone to fully cure on a heated 3D-printer bed maintained at 50 °C.

Black gel. The black gel is made from the same XP-565 silicone mixed with black pigment. After the transparent silicone cures, the upper mold (2) is removed and replaced by a second top mold (labeled 3 in Fig. 4(b)), which defines the perimeter volume allocated the black gel. Because this cavity is narrow and difficult to fill uniformly from above, we place an additional acrylic mold (labeled 4) on top of mold 3. The mixed black silicone is poured through the opening in mold 4 and flows into the perimeter cavity underneath it. This approach keeps the acrylic mold firmly pressed against the touching surface and ensures that the black gel cures to a uniform height around the transparent gel. After curing under the same heated-bed conditions, all molds are removed and excess gel around the fill opening is trimmed.

As indicated by label C in Fig. 4(b), the shell includes a small raised step along its perimeter. This feature creates the final three-layer edge profile (“shell–black gel–transparent gel”). The reason for this geometry is that mold 4 applies slight

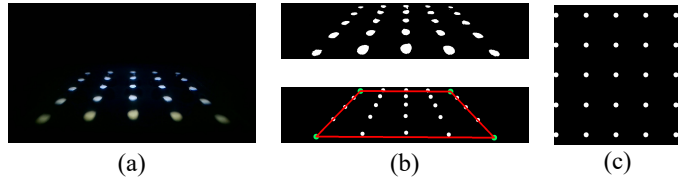


Figure 5. Camera calibration for LightTact. (a) LightTact captures imprints produced by a calibration tool with a 5×5 array of cylinders. (b) The imprints are segmented by thresholding and their center pixels are detected. (c) The final rectified and cropped image.

pressure on the transparent gel during the black-gel casting step. Once the molds are removed, the transparent gel relaxes back to its undeformed shape, which lifts the cured black gel upward by a small amount and leaves a thin air gap between the underside of the black gel and the top surface of the shell. Without the raised step on the shell perimeter, this air gap would open a direct lateral path for external light to enter the sensor and reach the camera. The raised perimeter therefore acts as a light-blocking barrier, preserving the “black surface” assumption required by our optical design.

D. Contact Segmentation

Camera operation and sensor calibration. The camera is set with auto-exposure *disabled* and uses a fixed exposure time of 20 ms during operation. This is crucial because auto-exposure would brighten the predominantly dark background of LightTact, amplifying sensor noise and potentially saturating bright contact regions. For robotic use, we additionally calibrate image pixels to their spatial positions on the touching surface. Following 9DTact [9], we design a calibration tool with a 5×5 array of cylindrical bumps at a spacing of 3 mm. As shown in Fig. 5(a), LightTact captures the imprint pattern when the tool is pressed onto the touching surface. We segment the imprints by simple thresholding and extract their center pixels (Fig. 5(b)). We then select the four outermost corner imprints in green to estimate the average pixel spacing, and compute the target rectified locations of all centers on an evenly spaced grid. Finally, using the correspondences between the detected centers and their rectified grid locations, we compute a warping map to rectify and crop each raw image to a top-down view (Fig. 5(c)).

Segmentation algorithm. The optical design of LightTact naturally produces a high-contrast representation of contact: non-contact regions remain near-black, while true contact results in localized brightness increases. Building on this property, our segmentation algorithm adopts a simple yet highly robust frame-differencing strategy. Before operation, LightTact records N no-contact frames and computes their pixel-wise average to form a stable reference image I_{ref} . For each incoming frame I , we compute a difference image $I_{\text{diff}} = I_{\text{raw}} - I_{\text{ref}}$, in which contact pixels appear as positive brightness changes. To reliably distinguish physical contact from sensor noise, we introduce a *multi-condition* brightness consistency check. A pixel at location (x, y) is classified as contact if any of the following four conditions is satisfied: (1)

Table II

INTENSITY STATISTICS AND REPRESENTATIVE IMAGES OF NON-CONTACT AND CONTACT CONDITIONS UNDER DIFFERENT INTERNAL AND EXTERNAL ILLUMINATION LEVELS.

| Internal brightness (Lux) | 0 | 430 | 1050 | 1670 | 430 | 430 | 430 | 430 | 430 |
|---------------------------|------|------|------|------|------|------|------|------|------|
| External brightness (Lux) | 3 | 3 | 3 | 3 | 740 | 1020 | 1510 | 2010 | 2540 |
| LightTact in environment | | | | | | | | | |
| Non-contact image mean | 0.41 | 1.00 | 1.79 | 4.26 | 1.28 | 1.52 | 2.40 | 2.94 | 4.69 |
| Non-contact image std | 0.49 | 0.33 | 0.97 | 3.45 | 0.47 | 0.64 | 1.09 | 1.61 | 2.83 |
| Non-contact raw image | | | | | | | | | |
| Contact raw image | | | | | | | | | |
| Contact segmentation | | | | | | | | | |

the mean RGB increase exceeds a threshold t_0 ; (2) at least one color channel exceeds threshold t_1 ; (3) at least two color channels exceed threshold t_2 ; or (4) all three color channels exceed threshold t_3 . These complementary conditions enable the algorithm to detect both prominent brightness changes and more subtle, consistent increases produced by contact. In our implementation, we use $N = 10$ and thresholds $\{t_0, t_1, t_2, t_3\} = \{25, 20, 30, 40\}$.

IV. EXPERIMENTS AND RESULTS

In this section, we conduct experiments to answer the following questions: 1) Can LightTact achieve the intended light-suppression behavior and produce natural high-contrast contact images? 2) Can LightTact perform robust deformation-independent contact segmentation across diverse materials, appearances, forces, and environment illumination? 3) What new manipulation capabilities does LightTact unlock when equipped on robots?

A. Light Suppression at Non-Contact Regions

We begin by evaluating whether LightTact achieves the intended light-suppression behavior under varying levels of internal illumination and external ambient brightness. We measure the brightness at the touching surface using a digital light meter. For each condition, we record (1) raw images without contact (non-contact images) and (2) raw images with a cylindrical object touching the sensing surface (contact images). We report the mean and standard deviation of the non-contact images in Table II, along with representative raw and segmented results.

Internal illumination. We first test LightTact in a dark environment and gradually increase the LED voltage. When the LED is off, both contact and non-contact images remain near-black as expected. As LED brightness increases to 430 Lux, the contact images begin to reveal clear visual appearance of the object while the non-contact regions remain

extremely dark (mean gray value = 1.0). Further increasing the LED brightness (e.g., 1050 or 1670 Lux) causes only slight increases in non-contact intensity. However, these higher illumination levels overexpose the contact regions and degrade object appearance. To maintain near-black non-contact regions and capture clear object appearance, we set 430 Lux (corresponding to a 3.4 V driving voltage) as the default internal illumination for LightTact.

External illumination. Using the default LED setting, we then increase external illumination by gradually brightening an external lamp. As shown in Table II, LightTact maintains its non-contact pixels near-black (mean gray value < 3) even under strong ambient lighting up to 2010 Lux, which is far above typical indoor brightness (< 1000 Lux). At extremely bright illumination conditions (3520 Lux), the non-contact image becomes slightly brighter (mean gray value = 6.90) due to imperfect absorption on the internal surfaces of the sensor, as discussed in Section III-B. Nonetheless, contact regions remain clearly visible and segmentation remains robust.

These results demonstrate that LightTact consistently suppresses both external and internal light at non-contact regions while preserving natural appearance in contact regions. This behavior directly validates our optical design and highlights a key distinction from TIR-based sensors [12, 13, 14, 15], which fail to distinguish contact regions under bright environments.

B. Deformation-Independent Contact Segmentation

Extremely light contact sensing. Figure 6 evaluates LightTact’s ability to detect contact from liquids (green juice, milk), semi-liquids (toothpaste), and ultra-soft materials (cotton, sponge, tofu, noodle, beef, fingertip, palm) under bright indoor lighting. All objects are placed or lightly touched onto the sensor without pressing, producing minimal or no macroscopic surface deformation. Despite this, LightTact reliably “sees” the contact region directly, and its optical light-suppression mechanism yields clean, pixel-level contact segmentation even

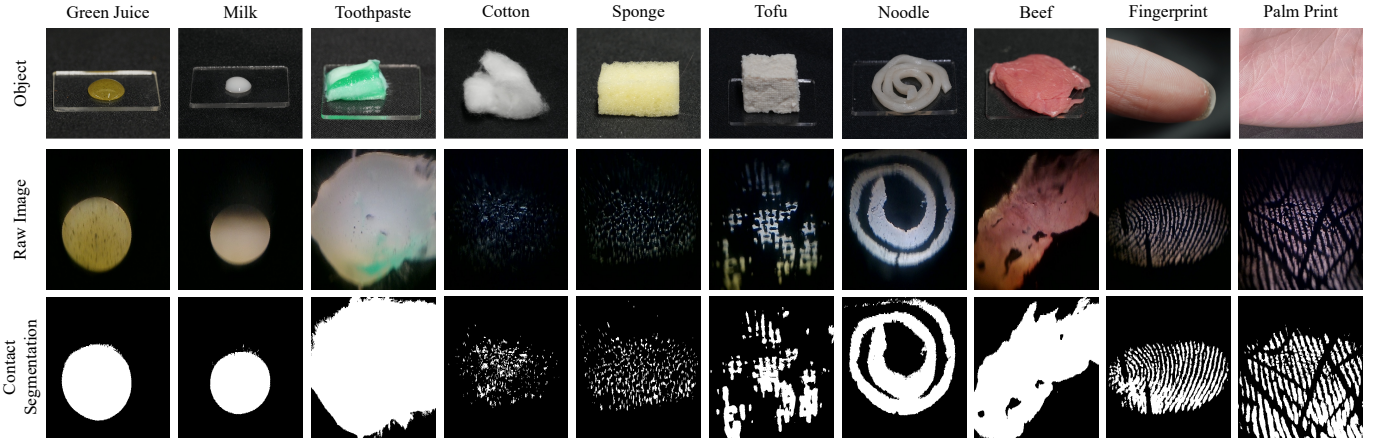


Figure 6. LightTact achieves robust contact segmentation with objects that make extremely light contact without producing macroscopic surface deformation, such as liquids, semi-liquids, and ultra-soft materials.

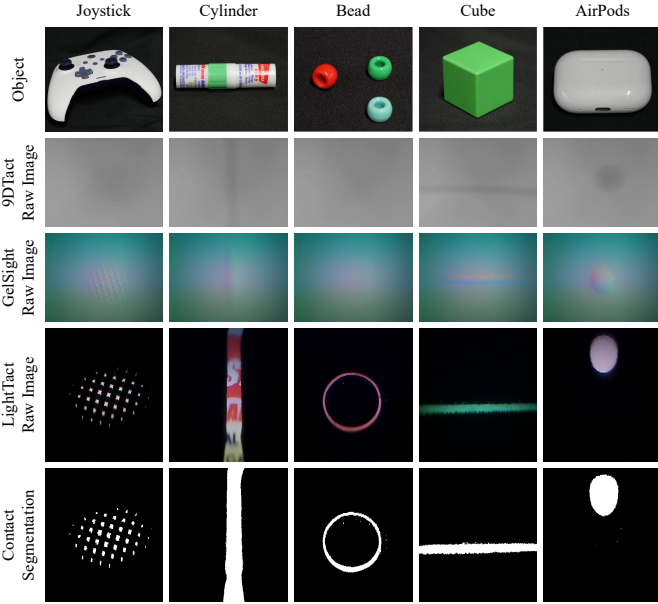


Figure 7. LightTact reliably senses both light and firm contact from rigid objects while preserving their visual appearance.

for objects with complex appearance. In contrast, 9DTact [9] and GelSight [7] fail to provide even binary contact detection under such light interactions, as their sensing fundamentally depends on measurable deformation. Moreover, LightTact can sense contact even under effectively zero applied force as demonstrated by the thin film hanging upside down on the downward-facing LightTact sensor in Fig. 1, indicating that LightTact does not require a minimum force threshold for detection.

Sensing across materials. Beyond liquids and soft materials, LightTact also provides robust visual-tactile sensing for rigid objects, as shown in Fig. 7 (textured joystick surface, complex-pattern cylinder, beads, cube, AirPods). Deformation-based VBTSSs sense only indentation and become ineffective under light contact, as illustrated by the bead example. In

contrast, LightTact consistently produces clean segmentation and natural visual appearance.

Together, these results demonstrate that LightTact reliably detects contact and performs accurate pixel-level segmentation across liquids, semi-liquids, ultra-soft materials, and rigid objects. This level of robustness to material properties, surface appearance, and environmental lighting is not achievable with TIR-based VBTSSs, and the multimodal richness is far beyond what deformation-based tactile sensors can provide.

C. Robotic Capabilities Unlocked by LightTact

To showcase the manipulation abilities enabled by LightTact’s direct, deformation-independent contact perception, we conduct a series of experiments on a UFACTORY xArm 7 robotic arm equipped with one or two LightTact modules mounted on its gripper. These demonstrations highlight two classes of capabilities:

- **Light contact sensing** for interaction with liquids, semi-liquids, and ultra-soft materials;
- **Multimodal reasoning** for fine-grained manipulation by directly prompting LightTact images to vision-language models (VLMs).

For all experiments, we additionally compare LightTact with a force-torque (FT) sensor and representative vision-based tactile sensors that are either open-source or commercially available, including 9DTact [9], GelSight-Mini [33], and DelTact [11]. We refer to these as *baseline sensors* below.

1) *Light contact sensing of liquids, semi-liquids, and soft materials:* When a robot approaches an object, the wrist camera view is often occluded, making tactile sensing essential for safe interaction. Materials without rigid boundaries (e.g., water and creams) and extremely soft or thin materials (e.g., food film) are particularly challenging for force-based and deformation-based tactile sensors because their contacts generate unmeasurable forces or microscopic deformation. In contrast, LightTact can directly detect such light contacts through its deformation-independent optical principle, enabling to unlock such light-contact interactions for robots.

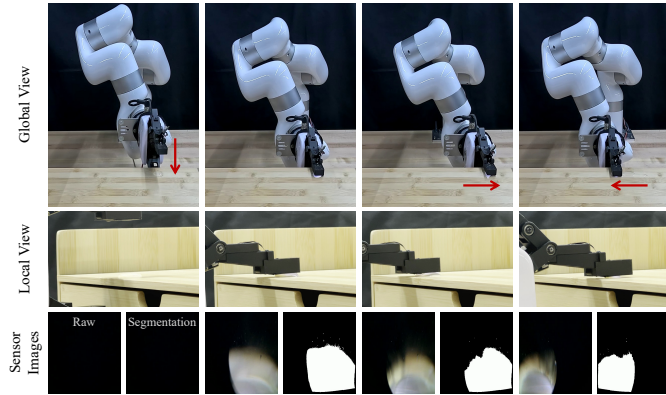


Figure 8. LightTact detects contact with water and segments the contact region, enabling the robot to spread water while maintaining contact and avoiding collision with the surface.

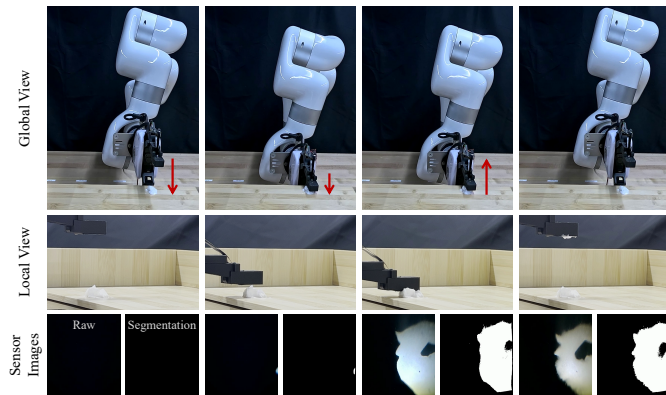


Figure 9. Using LightTact, the robot can dip facial cream using a contact-coverage criterion.

Liquid spreading. As shown in Fig. 8, a small amount of water is placed on a flat cabinet, and the robot orients LightTact downward. The gripper descends until contact is detected, then performs lateral sweeps while continuously adjusting its height to maintain contact with the water and avoid colliding with the surface. We regulate the end-effector height using a PD controller to maintain approximately 50% contact coverage. This closed-loop policy allows the robot to spread the water uniformly.

Semi-liquid dipping. As shown in Fig. 9, to collect facial cream, the robot moves its fingertip toward the cream, reduces its approach speed once contact is detected, and stops when more than 50% of the sensing surface is in contact. Notably, LightTact continues to detect the cream reliably during lifting, where essentially no pressure is applied on the sensing surface.

Extremely soft materials. As shown in Fig. 10, a human holds a small piece of food film that is ultra-soft, thin (0.1 mm), and light (0.05 g), and lightly touches it to a gripper equipped with two LightTact sensors. When the right sensor detects contact, the robot moves right; when the left sensor detects contact, it moves left; and when no contact is detected, it returns to a centered position. This behavior illustrates that LightTact can reliably sense minimal, delicate contacts and support responsive human-robot interaction.

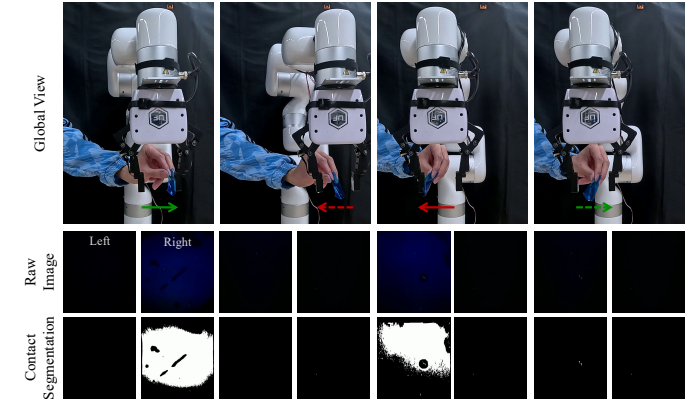


Figure 10. Two LightTact sensors enable responsive interaction with an ultra-thin film. Solid arrows indicate the end-effector motion commanded by contact on the corresponding sensor; dotted arrows indicate return to the centered position when no contact is detected.

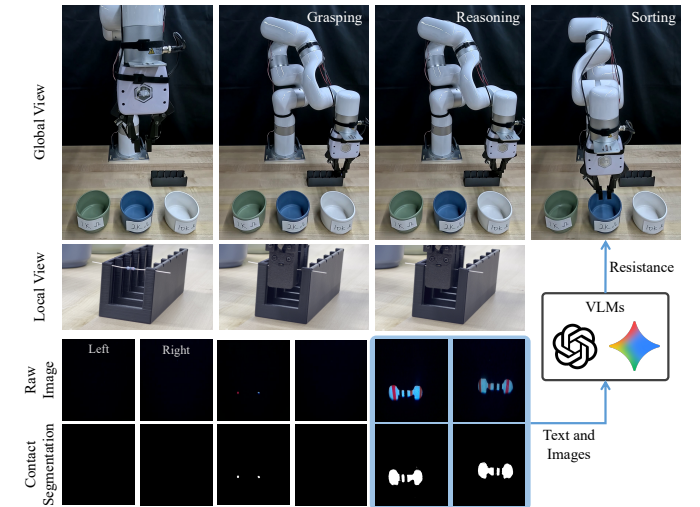


Figure 11. Beyond pixel-level contact sensing, LightTact preserves the natural appearance of the contacting surface, enabling VLMs to reason directly over its images. In this task, a VLM infers resistor values from color bands to guide robotic sorting.

Across all three tasks, the baseline sensors fail to produce usable signals because the contacts are too light to generate measurable forces or macroscopic deformation. These results underscore LightTact’s unique ability to enable robotic behaviors that require precise sensing of extremely light contact.

2) *Multimodal sensing and VLM-guided fine-grained manipulation:* Vision-language models (VLMs) are emerging as powerful general-purpose reasoning engines for robotics [34, 35]. However, conventional tactile inputs, either sparse force signals or deformation-based tactile images, provide limited appearance information and are often out-of-distribution for VLMs, making them difficult to interpret directly for manipulation [36, 37, 38]. In contrast, LightTact produces high-resolution, appearance-preserving images in which contact geometry and local object appearance are naturally aligned, making them directly compatible with VLM-based reasoning.

Resistor grasping and resistance reasoning. To demon-

strate this capability, the robot is tasked with grasping and sorting resistors by their resistance values. The gripper closes until one LightTact detects more than 100 contact pixels, yielding a stable and gentle grasp. We crop the raw image around the contact region and prompt a VLM (GPT-5 Pro in our implementation) to infer the resistance value from the color bands. The robot then places the resistor into the corresponding cup. We evaluate this pipeline over 20 trials with 5 resistors and achieve 16 successful sorts (80% success rate). Most failures arise from the VLM confusing visually similar band colors (e.g., red vs. brown vs. orange).

In contrast, the baseline sensors do not provide interpretable appearance cues and therefore cannot support this VLM-guided sorting pipeline. We also compare against wrist-camera images: the VLM fails consistently because the resistor occupies a small fraction of the image and the background is cluttered. Overall, these results demonstrate that LightTact can provide VLM-readable inputs without fine-tuning, enabling robots to obtain high-level task decisions directly through prompting.

V. CONCLUSION

We presented LightTact, a compact visual-tactile fingertip sensor that enables deformation-independent, optics-based contact sensing. The core idea is an ambient-blocking optical configuration that suppresses both external light and internal illumination at non-contact regions, while transmitting only the diffuse light generated at true contacts. This yields high-contrast raw images with near-black non-contact pixels and appearance-preserving contact pixels, making pixel-level contact segmentation simple and robust. Across systematic evaluations, LightTact maintains reliable contact segmentation over diverse materials (liquids, semi-liquids, ultra-soft materials, and rigid objects) and under strong ambient lighting. When integrated on a robotic arm, LightTact enables manipulation behaviors driven by extremely light contact, including water spreading, facial-cream dipping, and thin-film interaction, where force-based sensing and deformation-based VBTSSs fail. Moreover, LightTact provides spatially aligned visual-tactile images that can be directly prompted to vision-language models for fine-grained reasoning, demonstrated by resistor value inference for robotic sorting.

ACKNOWLEDGMENTS

We would like to thank Yuxiang Yang for his insightful discussions on sensor design and experiments throughout the project.

REFERENCES

- R. S. Dahiya, G. Metta, M. Valle, and G. Sandini, “Tactile sensing—from humans to humanoids,” *IEEE transactions on robotics*, vol. 26, no. 1, pp. 1–20, 2009.
- S. Luo, N. F. Lepora, W. Yuan, K. Althoefer, G. Cheng, and R. Dahiya, “Tactile robotics: An outlook,” *IEEE Transactions on Robotics*, 2025.
- H. Li, Y. Lin, C. Lu, M. Yang, E. Psomopoulou, and N. F. Lepora, “Classification of vision-based tactile sensors: A review,” *IEEE Sensors Journal*, 2025.
- S. Li, Z. Wang, C. Wu, X. Li, S. Luo, B. Fang, F. Sun, X.-P. Zhang, and W. Ding, “When vision meets touch: A contemporary review for visuotactile sensors from the signal processing perspective,” *IEEE Journal of Selected Topics in Signal Processing*, vol. 18, no. 3, pp. 267–287, 2024.
- Y.-H. Xin, K.-M. Hu, R.-J. Xiang, Y.-L. Gao, J.-F. Zhou, G. Meng, and W.-M. Zhang, “Vision-based tactile sensing: From performance parameters to device design,” *Applied Physics Reviews*, vol. 12, no. 2, 2025.
- K. He, “A survey of vision-based tactile sensors: Hardware, algorithm, application and future direction,” *IEEE Transactions on Instrumentation and Measurement*, 2025.
- W. Yuan, S. Dong, and E. H. Adelson, “Gelsight: High-resolution robot tactile sensors for estimating geometry and force,” *Sensors*, vol. 17, no. 12, p. 2762, 2017.
- A. Yamaguchi and C. G. Atkeson, “Combining finger vision and optical tactile sensing: Reducing and handling errors while cutting vegetables,” in *2016 IEEE-RAS 16th International Conference on Humanoid Robots (Humanoids)*. IEEE, 2016, pp. 1045–1051.
- C. Lin, H. Zhang, J. Xu, L. Wu, and H. Xu, “9dta: A compact vision-based tactile sensor for accurate 3d shape reconstruction and generalizable 6d force estimation,” *IEEE Robotics and Automation Letters*, vol. 9, no. 2, pp. 923–930, 2023.
- B. Ward-Cherrier, N. Pestell, L. Cramphorn, B. Winstone, M. E. Giannacini, J. Rossiter, and N. F. Lepora, “The tactip family: Soft optical tactile sensors with 3d-printed biomimetic morphologies,” *Soft robotics*, vol. 5, no. 2, pp. 216–227, 2018.
- G. Zhang, Y. Du, H. Yu, and M. Y. Wang, “Deltact: A vision-based tactile sensor using a dense color pattern,” *IEEE Robotics and Automation Letters*, vol. 7, no. 4, pp. 10 778–10 785, 2022.
- J. Y. Han, “Low-cost multi-touch sensing through frustrated total internal reflection,” in *Proceedings of the 18th annual ACM symposium on User interface software and technology*, 2005, pp. 115–118.
- K. Shimonomura, H. Nakashima, and K. Nozu, “Robotic grasp control with high-resolution combined tactile and proximity sensing,” in *2016 IEEE International Conference on Robotics and automation (ICRA)*. IEEE, 2016, pp. 138–143.
- S. Zhang, Y. Sun, J. Shan, Z. Chen, F. Sun, Y. Yang, and B. Fang, “Tirgel: A visuo-tactile sensor with total internal reflection mechanism for external observation and contact detection,” *IEEE Robotics and Automation Letters*, vol. 8, no. 10, pp. 6307–6314, 2023.
- Y. Sun, S. Zhang, Z. Chen, Z. Shen, F. Sun, C. Stefanini, D. Guo, S. Luo, J. Zhang, J. Shan *et al.*, “Soft contact simulation and manipulation learning of deformable objects with vision-based tactile sensor,” *IEEE Transactions on Automation Science and Engineering*, 2025.
- Pollen Robotics, “AmazingHand: Code and model to control the AH! (amazing hand),” <https://github.com/pollen-robotics/AmazingHand>, 2025, GitHub repository, accessed 2025-12-14.
- A. Alspach, K. Hashimoto, N. Kuppuswamy, and R. Tedrake, “Soft-bubble: A highly compliant dense geometry tactile sensor for robot manipulation,” in *2019 2nd IEEE International Conference on Soft Robotics (RoboSoft)*. IEEE, 2019, pp. 597–604.
- S. Cui, R. Wang, J. Hu, J. Wei, S. Wang, and Z. Lou, “In-hand object localization using a novel high-resolution visuotactile sensor,” *IEEE Transactions on Industrial Electronics*, vol. 69, no. 6, pp. 6015–6025, 2021.
- L. Zhang, Y. Wang, and Y. Jiang, “Tac3d: A novel vision-based tactile sensor for measuring forces distribution and estimating friction coefficient distribution,” *arXiv preprint arXiv:2202.06211*, 2022.
- S. Saga, H. Kajimoto, and S. Tachi, “High-resolution tactile sensor using the deformation of a reflection image,” *Sensor Review*, vol. 27, no. 1, pp. 35–42, 2007.
- S. Saga, R. Taira, and K. Deguchi, “Precise shape reconstruction by active pattern in total-internal-reflection-based tactile sensor,” *IEEE Transactions on Haptics*, vol. 7, no. 1, pp. 67–77, 2013.
- W. Wyman, “Method for optical comparison of skin friction-ridge patterns,” Aug. 17 1965, uS Patent 3,200,701.
- R. Greene, “The drawing prism: a versatile graphic input device,” in *Proceedings of the 12th annual conference on Computer graphics and interactive techniques*, 1985, pp. 103–110.
- F. R. Hogan, J.-F. Tremblay, B. H. Baghi, M. Jenkin, K. Siddiqi, and G. Dudek, “Finger-sts: Combined proximity and tactile sensing for robotic manipulation,” *IEEE Robotics and Automation Letters*, vol. 7, no. 4, pp. 10 865–10 872, 2022.
- Q. Wang, Y. Du, and M. Y. Wang, “Spectac: A visual-tactile dual-modality sensor using uv illumination,” in *2022 international conference*

on robotics and automation (ICRA). IEEE, 2022, pp. 10 844–10 850.

[26] W. Fan, H. Li, W. Si, S. Luo, N. Lepora, and D. Zhang, “Vitactip: Design and verification of a novel biomimetic physical vision-tactile fusion sensor,” in *2024 IEEE International Conference on Robotics and Automation (ICRA)*. IEEE, 2024, pp. 1056–1062.

[27] L. Luo, B. Zhang, Z. Peng, Y. K. Cheung, G. Zhang, Z. Li, M. Y. Wang, and H. Yu, “Compdvision: Combining near-field 3d visual and tactile sensing using a compact compound-eye imaging system,” in *2024 IEEE/RSJ International Conference on Intelligent Robots and Systems (IROS)*. IEEE, 2024, pp. 262–268.

[28] N. H. Nguyen, N. M. D. Le, Q. K. Luu, T. T. Nguyen, and V. A. Ho, “Vi2tap: A cross-polarization based mechanism for perception transition in tactile-proximity sensing with applications to soft grippers,” *IEEE Robotics and Automation Letters*, 2025.

[29] Y. Li, Y. Chen, Z. Zhao, P. Li, T. Liu, S. Huang, and Y. Zhu, “Simultaneous tactile-visual perception for learning multimodal robot manipulation,” *arXiv preprint arXiv:2512.09851*, 2025.

[30] F. R. Hogan, M. Jenkin, S. Rezaei-Shoshtari, Y. Girdhar, D. Meger, and G. Dudek, “Seeing through your skin: Recognizing objects with a novel visuotactile sensor,” in *Proceedings of the IEEE/CVF winter conference on applications of computer vision*, 2021, pp. 1218–1227.

[31] E. Roberge, G. Forney, and J.-P. Roberge, “Stereotac: A novel visuotactile sensor that combines tactile sensing with 3d vision,” *IEEE Robotics and Automation Letters*, vol. 8, no. 10, pp. 6291–6298, 2023.

[32] S. Athar, G. Patel, Z. Xu, Q. Qiu, and Y. She, “Vistac toward a unified multimodal sensing finger for robotic manipulation,” *IEEE Sensors Journal*, vol. 23, no. 20, pp. 25 440–25 450, 2023.

[33] GelSight. (2022) Gelsight-mini. [Online]. Available: <https://www.gelsight.com/gelsightmini/>

[34] J. Gao, B. Sarkar, F. Xia, T. Xiao, J. Wu, B. Ichter, A. Majumdar, and D. Sadigh, “Physically grounded vision-language models for robotic manipulation,” in *2024 IEEE International Conference on Robotics and Automation (ICRA)*. IEEE, 2024, pp. 12 462–12 469.

[35] G. R. Team, S. Abeyruwan, J. Ainslie, J.-B. Alayrac, M. G. Arenas, T. Armstrong, A. Balakrishna, R. Baruch, M. Bauza, M. Blokzijl *et al.*, “Gemini robotics: Bringing ai into the physical world,” *arXiv preprint arXiv:2503.20020*, 2025.

[36] S. Yu, K. Lin, and H. Soh, “Demonstrating the octopi-1.5 visual-tactile-language model,” *arXiv preprint arXiv:2507.09985*, 2025.

[37] J. Huang, S. Wang, F. Lin, Y. Hu, C. Wen, and Y. Gao, “Tactile-vla: Unlocking vision-language-action model’s physical knowledge for tactile generalization,” *arXiv preprint arXiv:2507.09160*, 2025.

[38] Z. Cheng, Y. Zhang, W. Zhang, H. Li, K. Wang, L. Song, and H. Zhang, “Omnivtla: Vision-tactile-language-action model with semantic-aligned tactile sensing,” *arXiv preprint arXiv:2508.08706*, 2025.

APPENDIX

A. Camera Placement under $\theta_{tv} < 2\theta_c$

In this section, we discuss our motivation to design the angle between the touching and viewing surfaces θ_{tv} . The optical objective is to prevent the camera from seeing external light from non-contact regions of the touching surface. To achieve this, we choose $\theta_{tv} = \frac{\pi}{2} > 2\theta_c$ for LightTact (Section. III) so that these rays meet TIR when they reach the viewing surface and cannot transmit through it.

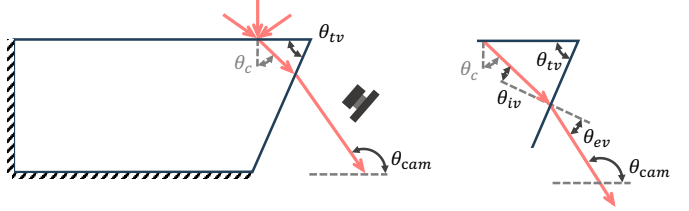


Figure 12. Optical analysis for the transparent medium under $\theta_{tv} < 2\theta_c$. External light can transmit through the viewing surface so the camera should be placed outside the areas where external light can arrive.

Another more relaxed design is to allow these rays to transmit through the viewing surface but with the camera outside the ray field. This choice allows $\theta_{tv} < 2\theta_c$ as illustrated in Fig. 12. In this situation, ambient light first transmits through the touching surface and reach the viewing surface. The incident angle has a maximal value of $\theta_{iv} = \theta_{tv} - \theta_c$. And the corresponding minimal exit angle is

$$\begin{aligned} \theta_{ev} &= f(\theta_{iv}) \\ &= \sin^{-1}\left(\frac{n_m}{n_a} \sin \theta_{iv}\right) \end{aligned} \quad (1)$$

where n_m and n_a are the refractive index of the transparent medium (around 1.45) and the air (around 1.0). Therefore, the angle between the most slant ray and the horizontal line is

$$\begin{aligned} \theta_{cam} &= \frac{\pi}{2} + \theta_{tv} - \theta_{ev} \\ &= \frac{\pi}{2} + \theta_{tv} - \sin^{-1}\left(\frac{n_m}{n_a} \sin \theta_{iv}\right) \\ &= \frac{\pi}{2} + \theta_{tv} - \sin^{-1}\left(\frac{n_m}{n_a} \sin(\theta_{tv} - \theta_c)\right) \end{aligned} \quad (2)$$

To satisfy the optical objective of suppressing ambient-light, the camera must be placed outside the areas where these rays can arrive. This makes the camera be put upper and more right, strongly restricting the compactness of the sensor. For example, when $\theta_{tv} = \theta_c$, it makes $\theta_{iv} = \theta_{ev} = 0$ and $\theta_{cam} = f(\theta_{iv}) = \frac{\pi}{2} + \theta_c$. In addition, to avoid these rays being reflected into the camera again, special design, such as matte-black surfaces, is required for the container (mount) of the camera. Therefore, to ensure more reliable satisfaction of the optical objective and more compact design, we finally choose $\theta_{tv} > 2\theta_c$ for LightTact.

B. Design of Sensor Components

We provide more rendered views of the sensor shell, transparent gel and black gel in Fig. 13.



Figure 13. Detailed views of the sensor shell, transparent gel and black gel.

C. Optical Analysis with Wedge Shape ($\theta_s < \frac{\pi}{2}$)

For certain robotic applications, LightTact may benefit from a wedge-shaped profile to access cluttered or confined spaces. To study the optical implications, we design and fabricate four wedge-shaped LightTact variants with different shell angles θ_s , using the same fabrication procedure as the default design. Under a bright indoor environment (approximately 1000 Lux), we record non-contact images from each variant and report their grayscale mean and standard deviation in Table III.

Table III

WEDGE-SHAPED LIGHTTACT VARIANTS AND THE MEAN AND STANDARD DEVIATION OF THEIR NON-CONTACT IMAGES

| θ_s (°) | 45 | 40 | 35 | 30 |
|----------------|------|------|------|------|
| Shell | | | | |
| Mean | 2.10 | 2.47 | 2.91 | 3.20 |
| Std | 0.85 | 1.03 | 1.26 | 2.33 |

As θ_s decreases, the slanted internal shell surface becomes more likely to reflect ambient light (both external and internal) into directions that can enter the camera through non-contact regions, leading to a gradual increase in non-contact intensity. Nevertheless, even at $\theta_s = 30^\circ$, the non-contact images remain close to black (mean gray value < 4.0), indicating that the light-suppression property is largely preserved under moderate wedge shaping. If even darker non-contact images are desired, the slanted surface can be further improved by enhancing its absorptivity (e.g., applying higher-absorption black coating) or by adding micro-textures/light-trap patterns to reduce specular

reflections.

D. Large-Area Contact Sensing

Large-area contact, especially against flat surfaces, is often challenging for deformation-based VBTSSs because the resulting deformation is both slight and spatially uniform, yielding weak or ambiguous signals. As shown in Fig. 14, LightTact avoids this limitation since its deformation-independent, optics-based principle makes contact directly visible, allowing it to reliably detect and segment large-area contact on flat surfaces without requiring heavy pressing.

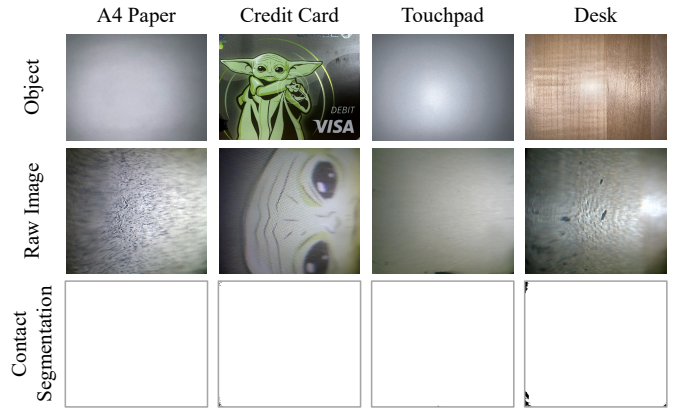


Figure 14. LightTact sensing large-area contact on flat surfaces. Unlike deformation-based VBTSSs, LightTact does not rely on measurable indentation and therefore remains effective even when contact is broad and deformation is minimal.

E. Details for Resistor Sorting

In the resistor sorting task, our text prompt to VLMs is:

The attached images are captured by two tactile sensors, which are mounted on the left and right side of a gripper. They are grabbing a resistor together. The tactile sensors can only see the part of the resistor that is contacting with the sensor's sensing surface. For the rest part of the sensing surface that is not in contact, the pixels remain black. The resistor has 5 bands that represent its resistance value. Please carefully analyze the 5 colors of the bands and compute the final resistance value of the resistor accurately. Notice that, read the color bands of the left sensor's image from left to right. Whereas read the color bands of the right sensor's image from right to left. Note that the internal illumination of the tactile sensor is relatively bright so be careful when inferring the colors. Please only output the final resistance value.